RSC Advances

PAPER

View Article Online
View Journal | View Issue

Cite this: *RSC Adv.*, 2024, **14**, 19459

Niobic acid as a support for microheterogeneous nanocatalysis of sodium borohydride hydrolysis under mild conditions†

Guilherme Mateus Bousada, [ac] Victor Nogueira da Silva,[a] Bárbara Fernandes de Souza,[a] Rodrigo Silva de Oliveira, [a] Iterlandes Machado Junior,[a] Carlos Henrique Furtado da Cunha,[b] Didier Astruc, [c] Robson Ricardo Teixeira [a] and Renata Pereira Lopes Moreira *[a]

This study explores the stabilization by niobic acid, of Pt, Ni, Pd, and Au nanoparticles (NPs) for the efficient microheterogeneous catalysis of $NaBH_4$ hydrolysis for hydrogen production. Niobic acid is the most widely studied Nb_2O_5 polymorph, and it is employed here for the first time for this key reaction relevant to green energy. Structural insights from XRD, Raman, and FTIR spectroscopies, combined with hydrogen production data, reveal the role of niobic acid's Brønsted acidity in its catalytic activity. The supported NPs showed significantly higher efficiency than the non-supported counterparts regarding turnover frequency, average hydrogen production rate, and cost. Among the tested NPs, PtNPs and NiNPs demonstrate the most favorable results. The data imply mechanism changes during the reaction, and the kinetic isotope assay indicates a primary isotope effect. Reusability assays demonstrate consistent yields over five cycles for PtNPs, although catalytic efficiency decreases, likely due to the formation of reaction byproducts.

Received 11th March 2024
Accepted 30th May 2024

DOI: 10.1039/d4ra01879f

rsc.li/rsc-advances

Introduction

Since the start of the Industrial Revolution, the increasing and extensive use of non-renewable energy sources has led to significant worldwide changes in the Earth's ecosystems.[1,2] Carbon-based energy sources, among which we find fossil fuels, emit highly harmful substances, including nitrogen oxides (NO_x) and sulfur oxides (SO_x), in addition to CO_2, which is the primary actor responsible for global warming.[3,4] In South America, for instance, since 2000, there has been a continuous increase in deaths from heat-related events among the elderly in almost all countries.[5] Moreover, emissions due to the burning of fossil fuels pose significant health risks, such as respiratory and cardiovascular issues.[6] Despite those challenges, modern society increasingly depends on energy consumption for its very survival.

Hydrogen has been envisioned as a viable alternative energy carrier that can replace fossil fuels and help reduce dependency on declining oil supplies while providing environmental and health benefits.[3,7,8] Indeed, depending on its source, hydrogen gas can be considered a carbon-neutral fuel, making it a promising candidate in the arsenal of strategies to slow down global warming.[8] However, despite those advantages, hydrogen gas is highly flammable, and its transport and storage present challenges in terms of economics and safety. These challenges arise from the requirement of high pressure, large vessel storage capacity, and substantial energy consumption to maintain low temperatures.[7–9] Another drawback is that most hydrogen currently produced comes from fossil fuels.[10]

To promote feasible and sustainable hydrogen production, extensive research has focused on water photosplitting/electroreduction and hydrogen evolution from inorganic hydrides.[10] Inorganic hydrides, such as boron hydrides like NH_3BH_3, $NaBH_4$, and $B_2(OH)_4$, are promising sustainable hydrogen storage systems.[7,10,11] These compounds are solid and stable at room temperature, ensuring safe storage. However, their hydrolysis reactions, although thermodynamically favorable, tend to be kinetically slow. Thus, utilizing catalysts is crucial to facilitate these reactions for efficient hydrogen production, enabling its application as a fuel.[12]

Among various inorganic hydrides, sodium borohydride ($NaBH_4$) stands out as one of the most studied, simplest, and hydrogen-rich chemical species for hydrogen production, theoretically releasing 4 mol of H_2 for every 1 mol of $NaBH_4$ hydrolyzed (eqn (1)).[7,12] It is a commonly used reducing agent in

[a]*Department of Chemistry, Universidade Federal de Viçosa, Viçosa, Minas Gerais, 36570-000, Brazil. E-mail: renata.plopes@ufv.br*

[b]*Department of Chemical Engineering, Universidade Federal de São Carlos, São Carlos, São Paulo, Brazil*

[c]*Institut des Sciences Moléculaires, Université de Bordeaux, UMR CNRS 5255, Talence 33405 Cedex, France*

† Electronic supplementary information (ESI) available. See DOI: https://doi.org/10.1039/d4ra01879f

both organic and inorganic chemistry,[13] being often employed to convert transition metal cationic salts into zero-valent metal nanoparticles when combined with a stabilizer,[14] or even acting as a metal nanocatalyst stabilizer itself.[15] The reduction of substrates by sodium borohydride can occur through both hydride transfer and single-electron transfer mechanisms due to its very cathodic redox potential.[13,16]

$$NaBH_{4(aq)} + 4H_2O_{(l)} \rightarrow NaB(OH)_{4(aq)} + 4H_{2(g)} \quad (1)$$

Although it slowly reacts with water to produce hydrogen gas, a reaction first recognized by Schlesinger,[17] this reaction is accelerated in the presence of transition-metal catalysts,[18] among which the use of metal nanoparticles (MNPs) is widespread.[19–22] These MNPs exhibit unique electronic properties due to quantum confinement and possess an enhanced surface/volume ratio, providing a greater number of active sites when compared to their bulk counterparts.[12] However, their high surface energy makes them prone to self-aggregation, leading to deactivation. To address this issue, various support materials have been proposed, including carbon-based structures, polymers, and metal–organic frameworks.[12,23,24] Notably, the use of niobium-based materials for this purpose has received limited attention in the literature, with no examples, to our knowledge, in sodium borohydride hydrolysis.

Niobium ($Z = 41$) is a group 5 transition metal, commonly found in nature alongside another element from the same group, tantalum ($Z = 73$).[25] This metal holds significant technological importance due to its extensive use in special alloys, being widely known for its exceptional superconducting properties.[26] Moreover, Nb has exhibited promising outcomes in catalyzing organic reactions, photocatalysis, and the creation of novel materials.[25,27–30]

The majority of the world's Nb reserves (>90%) are concentrated in Brazil, making it the dominant producer as well, accounting for *ca.* 93% of global production.[30] Investigations on Nb-catalyzed hydrogen production have used Nb in the form of complexes, combined with other metals, in the form of nanoparticles, and/or supported on other materials. Niobium-based semiconductors, for instance, are especially promising in hydrogen generation from water photosplitting reactions.[31,32]

Among niobium compounds, hydrated niobium pentoxide ($Nb_2O_5 \cdot nH_2O$), also known as niobic acid, is one of the most widely studied. Considering Nb_2O_5 polymorphs, it is the one with the highest acidity ($H_0 = -5.6$), despite its high water content, making it also stand out when compared to the acidity of other solids in general. It is an amorphous metal oxide composed mainly of distorted NbO_6 octahedra and NbO_4 tetrahedra. The highly polarized Nb–O bonds on its surface are responsible for some of the OH groups functioning as Brønsted acid sites. The Lewis acid sites, on the other hand, are mainly found within NbO_4 tetrahedra, which, even after the formation of NbO_4–H_2O adducts, retain effective positive charges. As a heterogeneous catalyst, it is insoluble in water, the holy grail green solvent, making it easily separable from the reaction medium and an interesting alternative for acid-driven reactions in aqueous media.[33–37]

Fraga *et al.*[37] demonstrated the exceptional efficiency of Nb_2O_5 as a support material for Pd, Ru, Co, and Ni in the pyrolysis reaction for oil upgrading through hydrodeoxygenation. This support led to a remarkable increase in activity, selectivity, and stability compared to other supports. Building upon these findings, our article reports the investigation of the microheterogeneous catalysis of $NaBH_4$ hydrolysis using MNPs stabilized by niobic acid.

Experimental

Standards and reagents

The experiments used sodium borohydride (NEON, CAS No. 16940-66-2), niobium pentoxide hydrated (Companhia Brasileira de Metalurgia e Mineração, CBMM), gold(III) chloride trihydrate (Sigma-Aldrich, CAS No. 16961-25-4), hexachloroplatinic(IV) acid hexahydrate (Sigma-Aldrich, CAS No. 18497-13-7), potassium tetrachloropalladate(II) (Sigma-Aldrich, CAS No. 10025-98-6), nickel(II) sulfate hexahydrate (Sigma-Aldrich, CAS No. 10101-98-1), acetone (Sigma-Aldrich, CAS No. 67-64-1), and isopropyl alcohol (Sigma-Aldrich, CAS 67-63-0). All reagents were used as received, without any further purification.

Synthesis of the catalysts

To synthesize AuNPs, PtNPs, PdNPs, and NiNPs, 34.45 μmol of a metal precursor (gold(III) chloride trihydrate, hexachloroplatinic(IV) acid hexahydrate, potassium tetrachloropalladate(II) or nickel(II) sulfate hexahydrate) was added to 10.0 mL of water and stirred for 15 min. After that, still under stirring, 1.00 mL of a 1.00 mol L^{-1} $NaBH_4$ solution was added to the system, and stirring continued for another 15 min. The precipitate was then separated by centrifugation at 4000 rpm for 15 min and washed three times with water, with intermediate centrifugations. The supernatant was removed, and the freshly prepared material was used as it was.

To synthesize AuNPs, PtNPs, PdNPs, and NiNPs supported on niobic acid, 34.45 μmol of a metal precursor (gold(III) chloride trihydrate, hexachloroplatinic(IV) acid hexahydrate, potassium tetrachloropalladate(II) or nickel(II) sulfate hexahydrate) was added to 10.0 mL of water containing 100 mg of niobic acid. The system was stirred for 15 minutes. After that, still under stirring, 1.00 mL of a 1.00 mol L^{-1} $NaBH_4$ solution was added to the system, and stirring continued for another 15 min. The solid was then separated by centrifugation at 4000 rpm for 15 min and washed three times with water, with intermediate centrifugations. The supernatant was removed, and the freshly prepared material was used as it was or dried under vacuum after washing with isopropyl alcohol or acetone.

To synthesize Ni : Pt bimetallic catalysts supported on niobic acid, 34.45 μmol of the metal precursors, nickel(II) sulfate hexahydrate and hexachloroplatinic(IV) acid hexahydrate, in varying molar proportions (80 : 20, 60 : 40, 40 : 60 or 50 : 50 Ni : Pt), was added to 10.0 mL of water containing 100 mg of niobic acid. The system was stirred for 15 minutes. After that, still under stirring, 1.00 mL of a 1.00 mol L^{-1} $NaBH_4$ solution was added to the system, and stirring continued for another 15 min.

The solid was then separated by centrifugation at 4000 rpm for 15 min and washed three times with water, with intermediate centrifugations. The supernatant was removed, and the freshly prepared material was used after drying under vacuum after washing with isopropyl alcohol or acetone.

Characterization

Fourier transform infrared (FTIR) spectroscopy. Attenuated total reflectance Fourier transform infrared (ATR-FTIR) analysis was performed on the samples using a VARIAN 660 FT-IR spectrophotometer (Varian, Palo Alto, CA, USA) equipped with GladiATR (480–4000 cm^{-1}).

Raman spectroscopy. Raman spectroscopy analysis was carried out using a micro-Raman Renishaw InVia spectrometer (Gloucestershire, England) equipped with a 50× Olympus BX41 objective lens and a Nd-YAG laser ($\lambda = 514$ nm). The acquisition time was set to 10 s.

X-ray diffraction (XRD). The samples were analyzed using a D8-Discover BRUKER instrument (Massachusetts, USA), with a copper tube ($\lambda = 1.5418$ Å), and sweeping over the range of $2\theta = 10$ to 80°, with a step size of 0.05°.

Transmission electron microscopy (TEM), energy dispersive X-ray spectroscopy (EDS), and selected area electron diffraction (SAED). Transmission Electron Microscopy (TEM) was employed to conduct morphological analysis. The analysis was carried out using a JEM-2100 Jeol Thermo Scientific microscope equipped with an Energy Dispersive X-ray Spectrometer (EDS) and a Tecnai G2-20-SuperTwin FEI-200 kV model device with a Si–Li detector (EDAX) for EDS. Samples were dispersed in an aqueous medium, and then a portion was deposited onto copper grids and coated with carbon film (Formvar). The EDS analysis was performed using a silicon drift detector with a resolution of 133 eV. The average size of the nanoparticles was determined using the ImageJ software, based on the average size of 40 nanoparticles.

Surface area analysis (BET) and pore size distribution (BJH). The nitrogen adsorption and desorption isotherms of the samples were determined using a Nova 600 Series (Anton Paar) instrument. Before the measurements, the sample underwent vacuum drying at 90 °C and 180 °C for 4 h to eliminate residual water and gases. The surface area was assessed using the Brunauer–Emmett–Teller (BET) method, and the pore size distribution was analyzed using the Barrett–Joyner–Halenda (BJH) method.

Thermogravimetric analysis. Thermogravimetric analysis was conducted using PerkinElmer's Simultaneous Thermal Analyzer 6000. Niobic acid was pre-weighed and then heated from room temperature to 900 °C at a rate of 10 °C min^{-1}. From the analysis the number of hydration water molecules was also calculated using stoichiometry.

Microwave-induced plasma atomic emission spectroscopy (MIP-AES). The quantification of the amount of incorporated metal on niobic acid (AuNPs, PtNPs, PdNPs, and NiNPs) was performed using microwave-induced plasma atomic emission spectroscopy (model 4100 MP-AES, Agilent Technologies, Australia) after digestion with aqua regia.

Sodium borohydride hydrolysis reaction. For the evaluation of the catalytic performance of the support, 100 mg of the support was added to a 125 mL Kitasato flask containing 20 mL of type II+ water. The flask was closed with a septum and coupled to a water-filled burette. The mixture was continuously stirred before adding, through a syringe, 1 mL of a freshly prepared aqueous solution containing 0.5 mmol of $NaBH_4$. The volume of hydrogen gas produced was determined by measuring the water displacement in the burette. The reactions were performed at room temperature.

For the evaluation of the catalytic performance of the support after heat treatment, the same procedure was repeated with 100 mg of niobic acid or niobic acid after heating at 300, 400, or 500 °C for 2 h. The reactions were performed at room temperature.

To evaluate the catalytic performance of the metallic nanoparticles or the metallic nanoparticles on niobic acid, the identical experimental protocol was employed using the freshly prepared catalysts described in Synthesis of the catalysts. The reactions were performed at room temperature.

To evaluate the catalytic performance of the PtNPs and NiNPs on niobic acid in the presence of sodium hydroxide, the same procedure was replicated with some adjustments: the Kitasato flask was substituted with a 10 mL Schlenk flask, and the volume of water was replaced with 1 mL of aqueous sodium hydroxide solutions (0.000, 0.010, 0.050, 0.100, or 0.200 mol L^{-1}) (Fig. S1†). Additionally, a 1 mL freshly prepared solution (using the sodium hydroxide solution as the solvent) containing 0.5 mmol of $NaBH_4$ was introduced into the system. The reactions were conducted at room temperature. The catalyst was previously vacuum-dried after being washed with isopropyl alcohol.

The same procedure described for the reactions in the presence of sodium hydroxide was used for bimetallic catalysts, substituting sodium hydroxide solution for type II+ water.

All reactions were performed until there was no visible displacement of water. The conversion of hydrogen volume to the amount of substance is described in detail in the ESI.†

Kinetic isotope effect assay

To evaluate the mechanism of the catalytic reaction of the support with Pt nanoparticles, the catalyst, synthesized as described previously, was washed with isopropyl alcohol or acetone and then vacuum-dried. Subsequently, it was added to a 10 mL Schlenk flask. To the flask, either 1 mL of type II+ water or 1 mL of deuterated water was added. The flask was closed with a septum and connected to a water-filled burette. The mixture was continuously stirred before introducing, through a syringe, 1 mL of a freshly prepared aqueous solution containing 0.5 mmol of $NaBH_4$ or 1 mL of a freshly prepared solution containing 0.5 mmol of $NaBH_4$ in deuterated water. The volume of hydrogen gas produced was determined by measuring water displacement in the burette. The reactions were performed at room temperature.

To ascertain the kinetic isotope effect (KIE),[38] the rate constant for each reaction was calculated as described in the ESI,† focusing on the most significant kinetic region.

Reusability assay

To assess the reusability of the PtNPs and NiNPs-supported catalysts, the catalyst, synthesized following the previously described procedures, was first washed with acetone and dried under vacuum. Next, it was added to a 10 mL Schlenk flask. To this flask, 1 mL of type II+ water was added. The flask was sealed with a septum and connected to a water-filled burette. The mixture was continuously stirred, and then 1 mL of a freshly prepared aqueous solution containing 0.5 mmol of $NaBH_4$ was introduced through a syringe. After the reaction, the catalyst was removed, thoroughly washed with type II+ water, and then centrifuged. The supernatant was discarded, and the catalyst was again washed with acetone and vacuum-dried. This reusability process was repeated for a total of 5 reactions. All reactions were performed at room temperature.

Results and discussion

Characterization

$Nb_2O_5 \cdot nH_2O$ is well-known for its significant Brønsted acidity due to the release of protons from hydroxyl groups attached to Nb and coordinated water molecules at NbO_4 sites.[33–35] However, this Brønsted acidity decreases as the material undergoes dehydration with increasing temperatures. This decrease in Brønsted acidity can be accompanied by the emergence of Lewis acid sites, resulting from inherent structural deficiencies.[35]

The dehydration process of $Nb_2O_5 \cdot nH_2O$ is evidenced in the infrared spectrum in Fig. 1a. Upon subjecting $Nb_2O_5 \cdot nH_2O$ to temperature treatments at 300, 400, and 500 °C, the O–H stretching band ($\nu_{O-H} = \sim 3250\ cm^{-1}$) and the H–O–H scissoring bend ($\delta_{H-O-H} = \sim 1620\ cm^{-1}$) disappear.[39] Additionally, Fig. 1a reveals other important bands, unrelated to the dehydration process, such as the Nb(–)(=)O stretching bands at ~480–900 cm^{-1}.[39b] The thermogravimetric analysis (Fig. 1b) also confirms the water loss, with more than a 10% decrease in the mass of niobic acid at temperatures above 500 °C due to the release of water molecules. Using this same analysis, the hydration of Nb_2O_5 was estimated as 1.4 ($Nb_2O_5 \cdot 1.4H_2O$).

The expected decrease in Brønsted acidity following dehydration was confirmed for the heat-treated niobic acid, as shown in Table 1. The heat-treated counterparts release fewer protons into the medium, as evidenced by the observed change in pH. In particular, niobic acid releases 2.6 times more protons into the medium after 10 min of stirring than its heat-treated counterpart at 500 °C.

The dehydration process also led to a surface area reduction in niobic acid, as indicated in Table 2, and the adsorption isotherms in Fig. 1c. Specifically, there was a 52% decrease in surface area when comparing the original material to the material treated at 500 °C. A transition from an amorphous phase (Fig. S2† and 1d) to a more crystalline structure (Fig. 1d) also evidenced the dehydration, as suggested in the literature.[33,35]

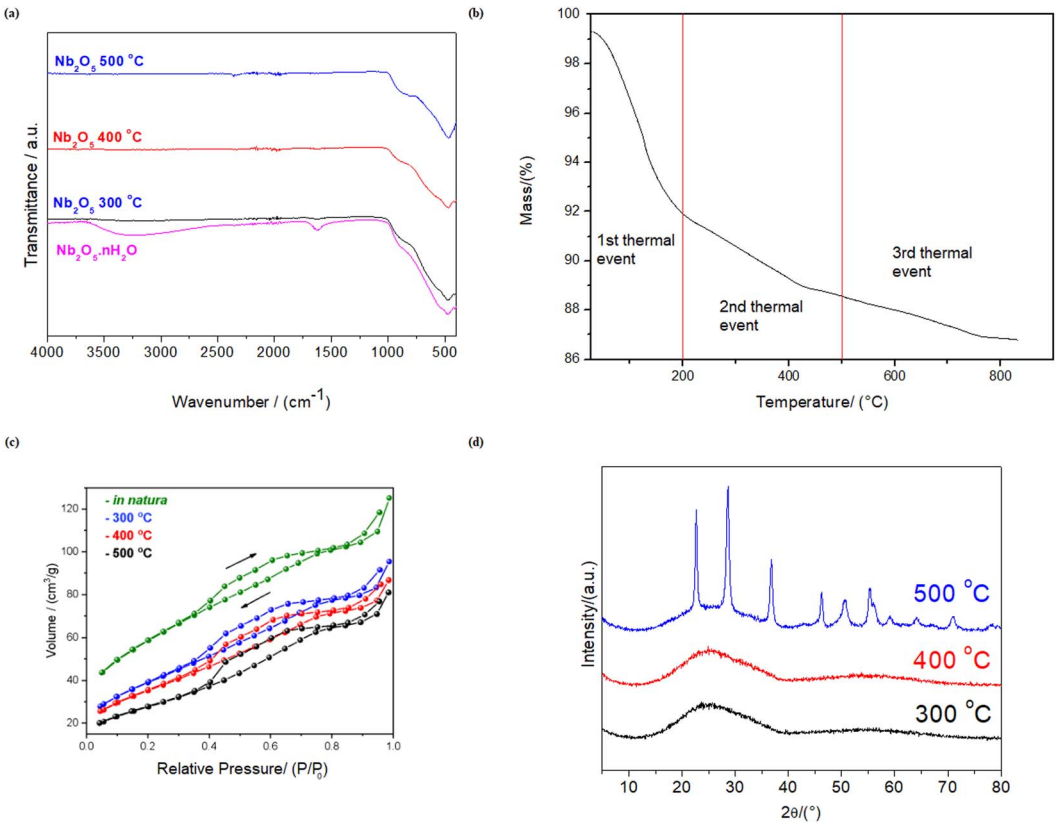

Fig. 1 (a) Infrared spectrum of niobic acid before and after heat treatment at 300, 400, and 500 °C. (b) XDR spectra of niobic acid after heat treatment at 300, 400, and 500 °C. (c) Adsorption isotherms for niobic acid and its heat-treated counterparts. (d) Thermogravimetric spectrum of niobic acid (30–900 °C).

Table 1 pH of 21 mL of water with 100 mg of niobic acid or its heat-treated counterparts after 10 min of stirring

$Nb_2O_5 \cdot nH_2O$ subjected to different types of heat treatment	pH
In natura	4.46
300 °C	4.53
400 °C	4.58
500 °C	4.88

The deposition of the metal nanoparticles was confirmed through analysis of the EDS spectra (Fig. S3†), TEM images (Fig. 2 and S4†), and MIP-OES data (Table 3). In addition to niobium and oxygen, sodium (resulting from the synthesis process) and silicon (niobic acid impurity) were also detected alongside the respective nanoparticles. The nanoparticles exhibited a well-dispersed spheroidal shape on the amorphous niobic acid sheets, with average sizes of 5.0 nm for NiNPs, 3.5 nm for PtNPs, 4.2 nm for PdNPs, and 6.1 nm for AuNPs. The

Table 2 Specific surface area of niobic acid and heat-treated counterparts

$Nb_2O_5 \cdot nH_2O$ subjected to different types of heat treatment (2 h)	Specific surface area ($m^2\ g^{-1}$)	Pore diameter (nm)	Pore volume ($cm^3\ g^{-1}$)
In natura	207.010	3.07137	0.118103
300 °C	141.243	3.45078	0.111984
400 °C	127.009	3.44728	0.102673
500 °C	99.977	3.44803	0.11234

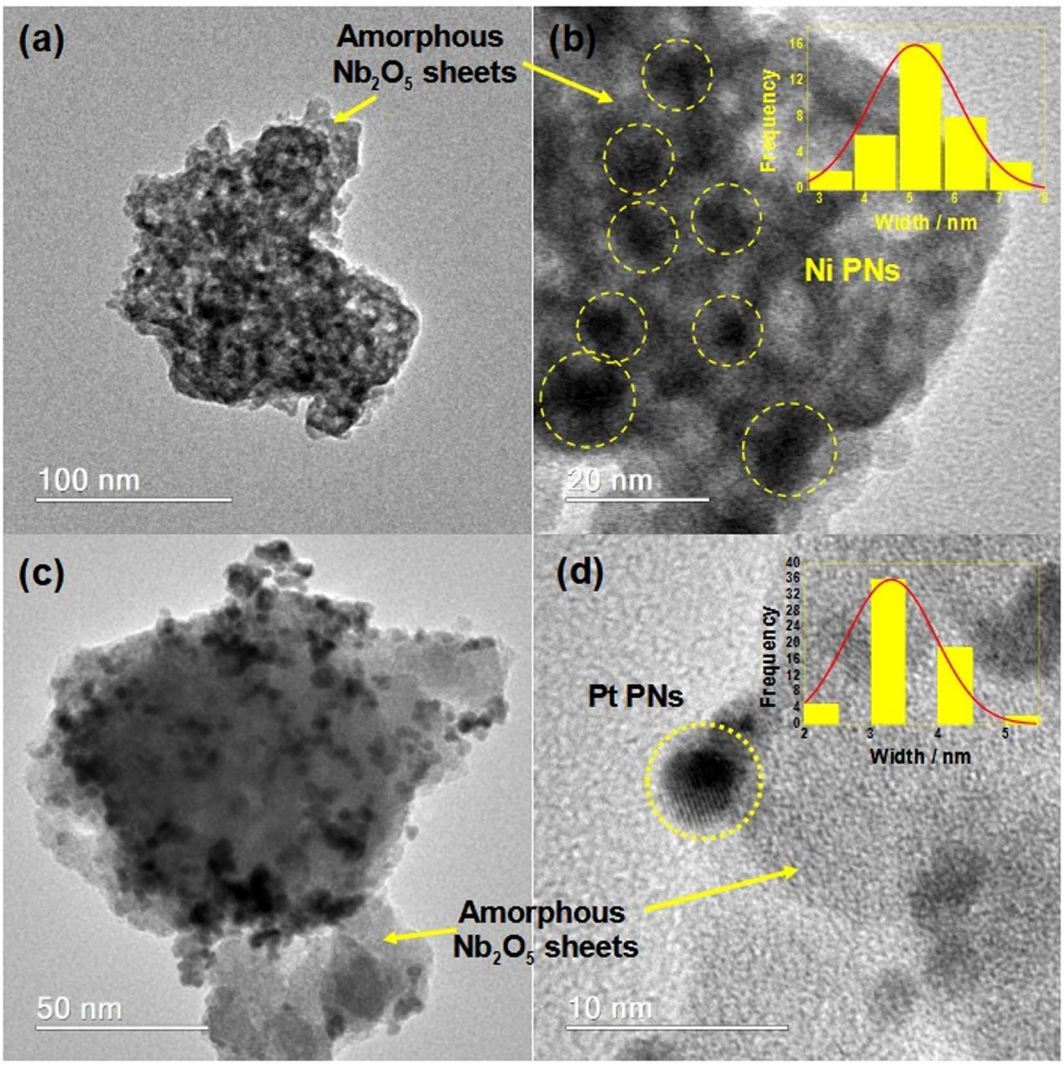

Fig. 2 TEM images of the (a and b) NiNPs/$Nb_2O_5 \cdot nH_2O$, inset: NiNPs size distribution. (c and d) PtNPs/$Nb_2O_5 \cdot nH_2O$, inset: PtNPs size distribution.

Table 3 Comparison between the catalyst performance of niobic acid-supported and non-supported nanoparticles

Catalyst	H_2 yield/(%)	Average rate[a]/(μmol_{H_2} min^{-1})	Metal loading[b]/(μmol)	TOF[c]/($mmol_{H_2}$ mol_{metal}^{-1} min^{-1})	Cost for hydrogen production[d]/(US$ per $mmol_{H_2}$ min)
PtNPs	67	93.6	34.45	6927	48.95
PtNPs/$Nb_2O_5 \cdot nH_2O$	69	1577.7	16.71	228 786	2.82
NiNPs	58	51.4	34.45	2397	0.37
NiNPs/$Nb_2O_5 \cdot nH_2O$	73	240.7	26.62	13 368	0.06
PdNPs	44	50.6	34.45	1895	39.97
PdNPs/$Nb_2O_5 \cdot nH_2O$	35	119.3	28.13	6063	21.31
AuNPs	5	6.3	34.45	290	7460.32
AuNPs/$Nb_2O_5 \cdot nH_2O$	10	17.8	23.32	1157	1320.22

[a] Total hydrogen produced/time. [b] Determined by MIP-OES analysis for the supported NPs. [c] TOF = derivative of the first linear range of H_2 production in the reaction/(metal loading). The first linear range corresponds to the linear equation obtained with $R^2 \geq 0.99$. [d] Cost = (price of the metal used in the synthesis)/(hydrogen yield × average rate).

interlamellar average distances measured were 0.221 nm for NiNPs, 0.153 nm for PtNPs, 0.291 nm for PdNPs, and 0.174 nm for AuNPs. The selected area electron diffraction (SAED) pattern of the NPs shown in Fig. S5† confirmed their crystalline nature. Furthermore, Fig. S6† illustrated the relationship between pore size and volume for all the NPs supported on niobic acid, revealing only marginal differences in pore size and surface area, except for the composite NiNPs/$Nb_2O_5 \cdot nH_2O$, which exhibited a considerably smaller surface area.

Catalyzed hydrolysis of sodium borohydride by niobic acid and its heat-treated counterparts

The graph illustrating the hydrogen production for the reactions catalyzed by niobic acid and its heat-treated counterparts can be seen in Fig. 3. All materials produced hydrogen gas in higher yields than the reaction without a catalyst, as well as all the reactions were much faster (2 to 17 times faster). Despite having low activity, $Nb_2O_5 \cdot nH_2O$ is still significantly more active than its heat-treated counterparts: the reaction with niobic acid is approximately seven times faster, resulting in twice the hydrogen production compared to its counterpart treated at 500 °C.

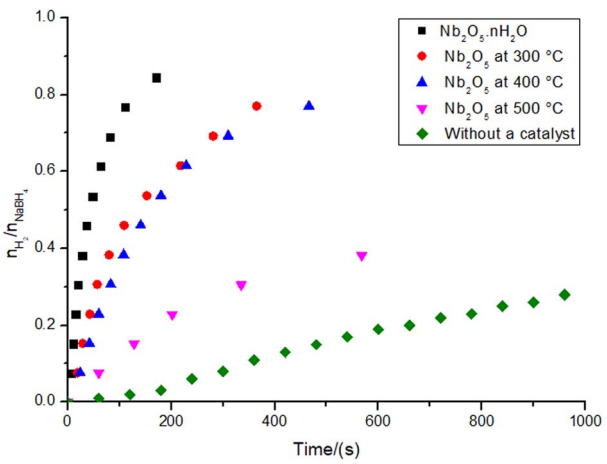

Fig. 3 Hydrogen production ratio with respect to the substrate (0.5 mmol of $NaBH_4$ in the final volume of 21 mL of type II+ water at 27.0 ± 1.0 °C) in the reactions catalyzed by 100 mg of niobic acid or its heat-treated counterparts (at 300, 400, and 500 °C).

Upon analyzing the structural insights provided in Fig. 1, the hydrogen production data in Fig. 3, and the variation in the system pH shown in Table 1, we can infer that the Brønsted acidity of $Nb_2O_5 \cdot nH_2O$ may play a role in its catalytic activity. This role can be accounted for by the acid-catalyzed hydrolysis of sodium borohydride (eqn (2)–(4)).

In acid catalysis, the borohydride anion reacts with a proton released or abstracted from niobic acid, liberating hydrogen gas and producing borane (eqn (2)). Then, borane is hydrolyzed, producing more hydrogen gas and boric acid (eqn (3)). Finally, boric acid is further hydrolyzed, generating a tetrahydroxyborate anion and liberating a proton (eqn (4)).[40]

$$BH_{4(aq)}^{-} + H_{(aq)}^{+} \rightarrow BH_{3(aq)} + H_{2(g)} \quad (2)$$

$$BH_{3(aq)} + 3H_2O_{(l)} \rightarrow B(OH)_{3(aq)} + 3H_{2(g)} \quad (3)$$

$$B(OH)_{3(aq)} + H_2O_{(l)} \rightarrow B(OH)_{4(aq)}^{-} + H_{(aq)}^{+} \quad (4)$$

The notable decrease in surface area and pore volume following thermal treatment should also be considered regarding the difference in activity as it may result in reduced accessibility of substrates to the catalyst surface.[33,37,41,42] This phenomenon was previously addressed in the discussion of Fig. 1d and Table 2.

Despite the reactions being conducted in water, the dehydrated materials do not rehydrate. This can be attributed to the rearrangement of amorphous $Nb_2O_5 \cdot nH_2O$ to the TT-Nb_2O_5 pseudohexagonal phase, as illustrated in Fig. 1d.[33,35] This

arrangement hinders the regeneration of Brønsted acidity even after water addition, leading to a decrease in the availability of OH groups. These groups are derived from both hydroxyl groups directly attached to Nb and water associated with NbO_4 tetrahedra.[33]

Catalyzed hydrolysis of sodium borohydride by metal nanoparticles (MNPs) over niobic acid

To further evaluate the performance of niobic acid in stabilizing the metal nanocatalysts, the transition metal salt precursors (gold(III) chloride trihydrate, hexachloroplatinic(IV) acid hexahydrate, potassium tetrachloropalladate(II), and nickel(II) sulfate heptahydrate) were reduced onto niobic acid. Fig. 4 illustrates the hydrogen production data for the nanocatalysts that were tested.

The first result that requires attention is the incomplete nature of the reactions. According to eqn (1), the hydrolysis of 1 mol of sodium borohydride should yield 4 mol of hydrogen gas. However, as depicted in Fig. 4, the highest $n\mathrm{H_2}/n\mathrm{NaBH_4}$ ratio observed was 3. This trend is consistent with findings from several other studies conducted at room temperature.[43–47]

There are several possible explanations for these results. First, the increase in the pH of the system, as expected for this reaction, may have helped to stabilize the unreacted starting material, slowing down the hydrolysis process enough to prevent it from completing within the time-frame of the experiment.[48] Second, at each hydrolysis step, when a hydroxyl group replaces the hydride, introducing an electron-withdrawing group makes it more challenging for a subsequent hydride transfer. In other words, the last hydride transfer of the final hydridic H atom of $B(H)(OH)_3$ has insufficient hydricity.[49]

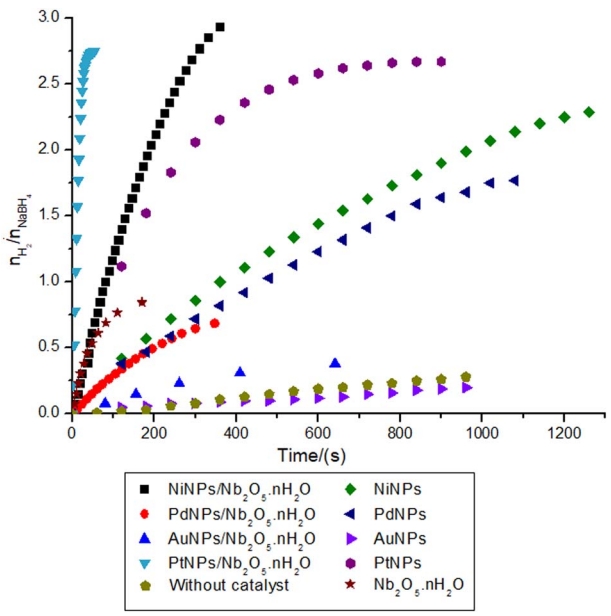

Fig. 4 Hydrogen production ratio with respect to the substrate (0.5 mmol of $NaBH_4$ in the final volume of 21 mL of type 1 water at 27.0 ± 0.5 °C) in the reactions catalyzed by niobic acid-supported and non-supported metal nanocatalyst (Ni, Pd, Au, or PtNPs).

Table 3 provides a performance comparison between metal nanoparticles (MNPs) and MNPs supported on niobic acid, with costs determined using the prices outlined in Table S1.† The findings indicate that the introduction of niobic acid, even with lower incorporation of nanoparticles, yielded significantly better turnover frequency (TOF), average hydrogen production rate, and cost than the non-supported nanoparticles.

Both AuNPs and PdNPs demonstrated unexpectedly low activity despite their potential in heterogeneous catalysis.[50–52] For instance, AuNPs/$Nb_2O_5\cdot n\mathrm{H_2O}$ exhibited a performance similar to niobic acid treated at 500 °C, the less acidic support, resulting in a final yield (9.6%) comparable to the reaction without any catalyst (7.0%). Interestingly, the infrared spectra of the composites AuNPs/$Nb_2O_5\cdot n\mathrm{H_2O}$ and PdNPs/$Nb_2O_5\cdot n\mathrm{H_2O}$ showed a higher absorption intensity for the band related to the O–H stretching (ν_{O-H} = ~3250 cm^{-1}) when compared with NiNPs/$Nb_2O_5\cdot n\mathrm{H_2O}$, PtNPs/$Nb_2O_5\cdot n\mathrm{H_2O}$, and $Nb_2O_5\cdot n\mathrm{H_2O}$ (Fig. S7†). These findings may suggest that a stronger interaction of AuNPs and PdNPs with OH groups inhibits the reaction, reinforcing the hypothesis that free OH groups in niobic acid contribute to the catalysis, as discussed for the Brønsted acidity. Additionally, the low activity of non-supported AuNPs and PdNPs and the infrared results suggest that these NPs may adsorb water more strongly, slowing the hydrolysis steps.

The top-performing catalysts, PtNPs/$Nb_2O_5\cdot n\mathrm{H_2O}$ and NiNPs/$Nb_2O_5\cdot n\mathrm{H_2O}$, saw a significant increase in turnover frequency (TOF): +3202% and +458%, respectively. There was also an increase in the average hydrogen production rate of +1586% and +368% respectively, along with a cost reduction of −94% and −84%. The costs presented in Table 3 were normalized based on average hydrogen production rates and reaction yields relative to the metal utilized in the synthesis. The most efficient catalysts also demonstrated the lowest costs, at 2.82 and 0.06 US$ per $mmol_{H_2}$ min for PtNPs and NiNPs, respectively. Even though the reaction with supported NiNPs is notably slower than the one with PtNPs, the significant difference in reagent price, depending on the intended application, still would favor Ni. A larger-scale synthesis or other engineering approaches could be utilized to circumvent this issue if needed. Except for PdNPs, supporting the NPs on niobic acid either did not impact the hydrogen yield or resulted in a significant improvement (such as a +26% increase for NiNPs).

Regarding the reactions with NiNPs/$Nb_2O_5\cdot n\mathrm{H_2O}$ and PtNPs/$Nb_2O_5\cdot n\mathrm{H_2O}$, the graphs in Fig. 5 depict the correlations between time and the test function ($F(C)$), which were used to determine the kinetic parameters for the reactions. The test function is a "mathematical trick" for the linearization of the analytical solutions for the differential equation used to describe the kinetics of the reactions (eqn (S3)–(S7)†). Refer to the ESI† for further details on how the test function was obtained.

At first glance, the data reveals significant differences in the reaction orders for both metals, suggesting distinct mechanisms. The hydrolysis of sodium borohydride by NiNPs/$Nb_2O_5\cdot n\mathrm{H_2O}$ approaches a pseudo-first-order reaction (n = 0.97), whereas the hydrolysis by PtNPs displays an unusual, higher-than-pseudo-fourth-order (n = 4.5).

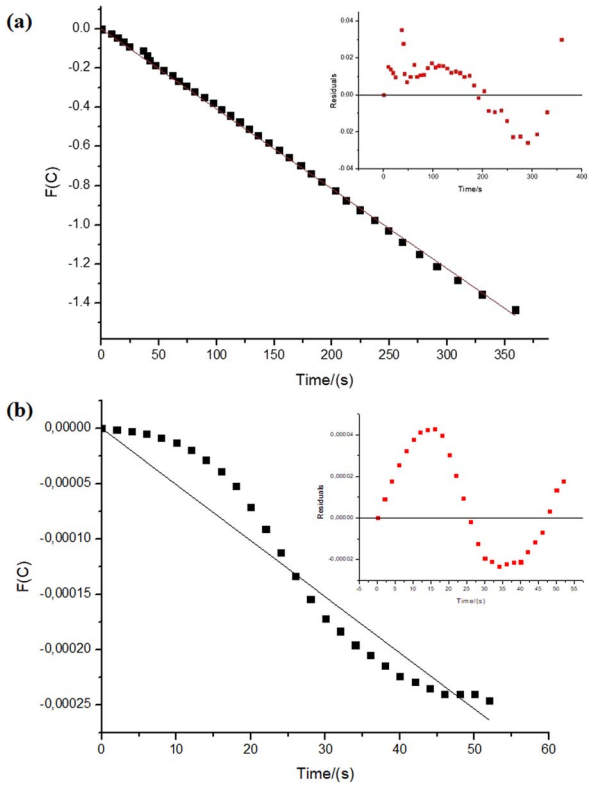

Fig. 5 Kinetic relations for sodium borohydride hydrolysis reactions (0.5 mmol of $NaBH_4$ in the final volume of 21 mL of type II+ water at 27.0 ± 0.5 °C). The intercepts were fixed at 0. In the insert: residuals plot. The parameters were obtained considering the variation in sodium borohydride's concentration (a) 34.45 μmol of NiNPs over 100 mg of niobic acid: $n = 0.97$ and $k = 0.048$ $mmol^{1-n}$ L^n s^{-1}, adjusted $R^2 = 0.9995$. (b) 34.45 μmol of Pt over 100 mg of niobic acid: $n = 4.5$ and $k = 5.1 \times 10^{-6}$ $mmol^{1-n}$ L^n s^{-1}, adjusted $R^2 = 0.9751$.

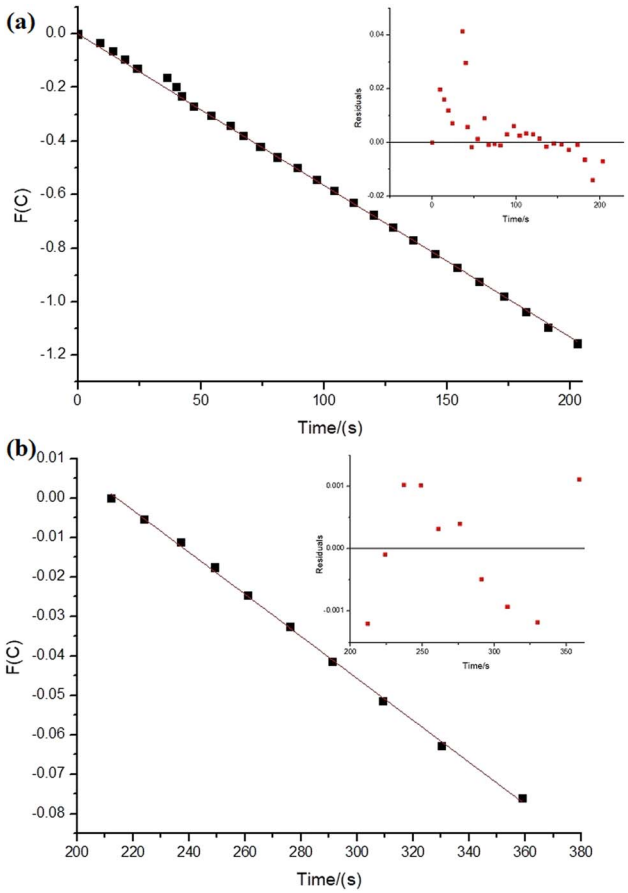

Fig. 6 Kinetic relations for sodium borohydride hydrolysis reactions (0.5 mmol of $NaBH_4$ in the final volume of 21 mL of type 1 water, 34.45 μmol of NiNPs over 100 mg of niobic acid at 27.0 ± 0.5 °C). In the insert: residuals plot. The parameters were obtained considering the sodium borohydride's concentration. (a) $n = 0.85$ and $k = 0.0057$ $mmol^{1-n}$ L^n s^{-1}, time 0 to 203 s, adjusted $R^2 = 0.9996$. (b) $n = 1.9$ and $k = 5.3 \times 10^{-4}$ $mmol^{1-n}$ L^n s^{-1}, time 212 to 259 s, intercept: 0.11, adjusted $R^2 = 0.9985$.

However, upon careful analysis of the graphs, the bias in the dispersion of the residuals (as seen in the inserts in Fig. 5a and b) becomes evident. This bias can be accounted for the concentration-dependent change in the mechanism of sodium borohydride hydrolysis, which can be influenced by various factors, including the reduction of water activity due to an increase in viscosity, and even the interference of the reaction intermediates.[40,53] Furthermore, mass transfer can become an issue in the relatively high amount of solvent used in the reaction. Therefore, we decided to examine the reaction considering different time-frames to understand better the possible changes in the hydrolysis mechanism (Fig. 6 and 7).

As depicted in Fig. 6, the reaction with $NiNPs/Nb_2O_5 \cdot nH_2O$ initially approaches a pseudo-first-order behavior with respect to sodium borohydride until 203 s of the reaction ($n = 0.85$), after which it transitions to a pseudo-second-order behavior until the completion of the reaction ($n = 1.9$). In contrast, the reaction with $PtNPs/Nb_2O_5 \cdot nH_2O$ (Fig. 7) exhibits a more complex behavior. It approaches a pseudo-zero-order reaction until 14 s ($n = 0.4$), followed by a pseudo-second-order reaction until 24 s ($n = 1.9$). After that, there are multiple mechanism changes along the time, suggested by high reaction orders ($n > 10$).

For the reaction with $PtNPs/Nb_2O_5 \cdot nH_2O$, after 34 s, the catalyst surface seems to undergo deactivation due to poisoning, caused by the formation of tetrahydroxyborate anions ($B(OH)_4^-$), leading to a leveling of the reaction rate.[7,54] This deactivation may explain the slightly lower yield for the hydrolysis promoted by $PtNPs/Nb_2O_5 \cdot nH_2O$ in comparison to the one promoted by $NiNPs/Nb_2O_5 \cdot nH_2O$. The deactivation of NiNPs might not have happened to the same extent as for PtNPs due to the differences in affinity of borates for the NPs' surface as well as the time required for borates transfer from the catalyst surface to the bulk phase of the reaction. In cases where the reaction proceeds rapidly, the available time for mass transfer decreases, enhancing the likelihood of poisoning.

Catalyzed hydrolysis of sodium borohydride by PtNPs over niobic acid in basic medium

There have been reports suggesting the use of sodium hydroxide in the reaction system to improve the performance of metal nanoparticles during the hydrolysis of $NaBH_4$. This

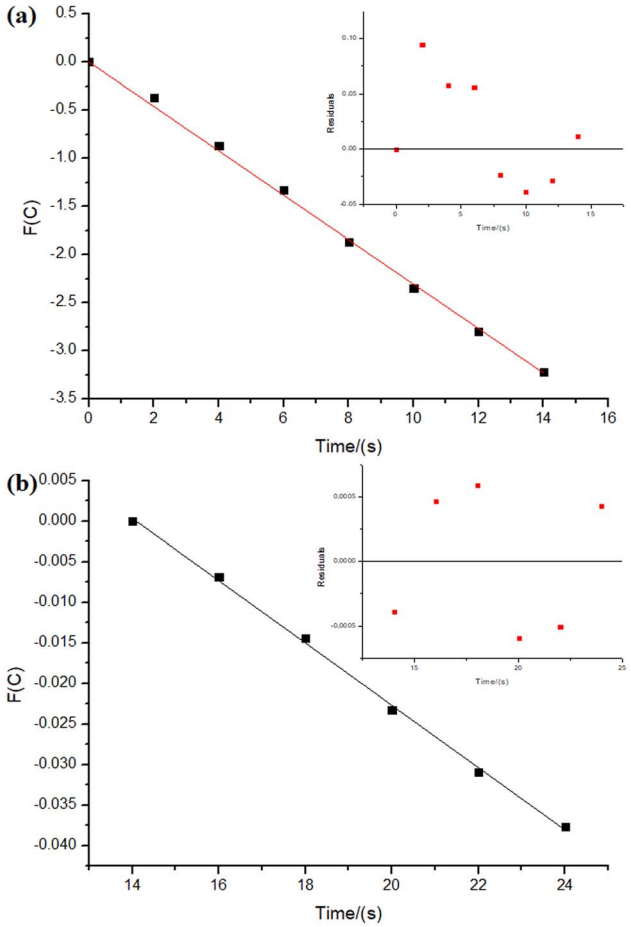

Fig. 7 Kinetic relations for sodium borohydride hydrolysis reactions (0.5 mmol of $NaBH_4$ in the final volume of 21 mL of type 1 water, 34.45 μmol of PtNPs over 100 mg of niobic acid at 27.0 ± 0.5 °C). In the insert: residuals plot. The parameters were obtained considering the sodium borohydride's concentration. (a) $n = 0.4$ and $k = 0.23$ $mmol^{1-n}$ L^n s^{-1}, time 0 to 14 s, adjusted $R^2 = 0.9993$. (b) $n = 1.9$ and $k = 3.8 \times 10^{-3}$ $mmol^{1-n}$ L^n s^{-1}, time 14 to 24 s, intercept: 0.054, adjusted $R^2 = 0.9982$.

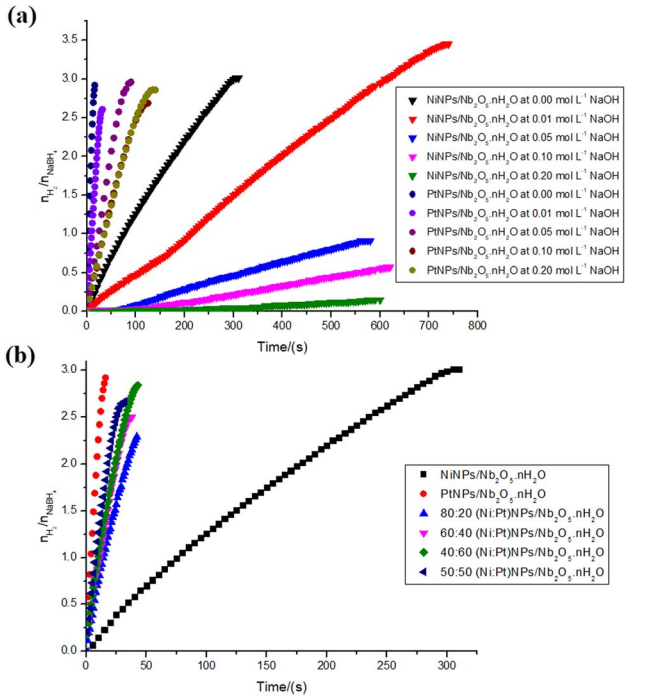

Fig. 8 Hydrogen production ratio with respect to the substrate: 0.5 mmol of $NaBH_4$ in the final volume of 2 mL of type II+ water (a) or sodium hydroxide solution at 0.050, 0.100, 0.200 mol L^{-1}. The reactions were catalyzed by 34.45 μmol of PtNPs or NiNPs over 100 mg of niobic acid at 23 ± 1 °C. (b) The reactions were catalyzed by 34.45 μmol of (Ni : Pt)NPs at different ratios (80 : 20, 60 : 40, 40 : 60, and 50 : 50) over 100 mg of niobic acid at 23 ± 1 °C.

improvement is attributed to the coordination of hydroxide anions onto the surface of the nanoparticles, resulting in an electron-rich surface. As a consequence, the oxidative addition of O–H, a typical step in metal-mediated sodium borohydride hydrolysis, is facilitated.[54]

To determine if this phenomenon is applicable in the current study, as well as to confirm the significance of the Brønsted acidity in the catalysis, the hydrolysis of sodium borohydride was carried out at varying concentrations of sodium hydroxide for the reactions catalyzed by $NiNPs/Nb_2O_5 \cdot nH_2O$ and $PtNPs/Nb_2O_5 \cdot nH_2O$, as illustrated in Fig. 8a. The reaction system was reduced to facilitate the experiments (from 21 mL to 2 mL size).

The observed difference in the average speed of the $PtNPs/Nb_2O_5 \cdot nH_2O$-catalyzed reaction (1577.7 μmol_{H_2} min^{-1} at 27 °C to 5053.8 μmol_{H_2} min^{-1} at 22 °C) and the $NiNPs/Nb_2O_5 \cdot nH_2O$-catalyzed reaction (240.7 μmol_{H_2} min^{-1} at 27 °C to 285.5 μmol_{H_2} min^{-1} at 22 °C), without the addition of sodium hydroxide, may be attributed to the higher concentration of sodium borohydride or the temperature increase during sodium borohydride hydrolysis.[55] It is worth noting that a smaller system resulted in similar hydrogen yields (73 and 75% for $PtNPs/Nb_2O_5 \cdot nH_2O$ and $NiNPs/Nb_2O_5 \cdot nH_2O$, respectively) and changed the costs for hydrogen production concerning the metal used in the catalyst synthesis: 0.83 and 0.014 US$ per $mmol_{H_2}$ min for Pt and NiNPs, respectively, representing cost reductions of −71% and −77%, respectively.

The ESI† provides details on the calculations for temperature variations, roughly estimated as 0.8 °C for the reaction in 21 mL, and 8.8 °C for the reaction in 2 mL of water (worst-case scenario, without any temperature control). This shows, as expected, that a higher amount of solvent plays a more effective role as a heat sink for the reaction. Even if the system's temperature is controlled by an oil bath, the combination of a short reaction time and a small solvent amount makes it plausible to assume the generation of heat spots that might influence the reaction speed.

Considering now the reactions in the presence of sodium hydroxide, it was shown that the higher the concentration of the base, the slower the kinetics for both nanoparticles tested. A set of different factors might lead to these results.

Firstly, for $PtNPs/Nb_2O_5 \cdot nH_2O$, the most active catalyst, the surface of PtNPs is already electron-rich. Instead of further enriching the surface with electrons, the coordination of hydroxide anions to the surface hinders the active sites.

Secondly, the increased viscosity of the reaction medium restricts the mass transfer of the reagent to the catalyst surface.[53,54] Additionally, the catalytic activity of niobic acid, as previously demonstrated, appears to be linked to its surface Brønsted acidity. Therefore, the higher basicity of the reaction mixture after the addition of sodium hydroxide reduces the catalytic activity of the support by decreasing the surface's Brønsted acidity. Besides, a more negative surface, linked to the consumption of protons, might also have hindered the approximation of the negatively charged borohydride ion. Finally, the essentially equal outcomes for the higher concentrations of NaOH may be explained by the saturation of the NPs' surface with hydroxide ions.

A similar pattern was found for NiNPs/$Nb_2O_5 \cdot nH_2O$, and the same reasons outlined above can account for this. However, there is one notable contrast: although both PtNPs/$Nb_2O_5 \cdot nH_2O$ and NiNPs/$Nb_2O_5 \cdot nH_2O$ yield essentially the same results when 2 mL of water (0.000 mol L^{-1} of NaOH) is used, the reaction with NiNPs showed a significant increase in yield when 0.01 mol L^{-1} of NaOH was utilized. This unexpected outcome remains to be explained.

Catalyzed hydrolysis of sodium borohydride by bimetallic NPs composites (Pt : Ni) over niobic acid

Trying to find a possible positive synergism between NiNPs and PtNPS, several bimetallic composites were synthesized with varying molar ratios: 80 : 20, 60 : 40, 40 : 60, and 50 : 50. As in the case of the reactions in basic medium, the experimental setup also involved the use of a lower amount of solvent (2 mL instead of 21 mL). The results for the performance of bimetallic composites over niobic acid are depicted in Fig. 8b.

When deposited onto a support, bimetallic catalysts can adopt various configurations, such as alloys, core–shell structures, or assume random orientations.[56] The interaction between metals can result in unique properties compared to monometallic catalysts due to synergistic effects.[56] In the current study, the presence of NiNPs had a negative impact on both the reaction speed and yield compared to PtNPs alone. Except for the most favorable bimetallic composite (50 : 50), an increase in the amount of NiNPs correlated with a decrease in the reaction speed. This observation can be attributed to factors such as non-cooperative electronic interactions, the potential blocking of the more active platinum surface by nickel, and/or the formation of inactive phases.[56]

Study on the reusability of PtNPs and NiNPs over niobic acid catalyst

To assess the reusability efficiency of NiNPs and PtNPs over niobic acid in the hydrolysis of sodium borohydride, a series of reactions were conducted. The catalyst was washed and vacuum-dried before each reaction cycle. The results are presented in Fig. 9.

As shown in Fig. 9a, there was no significant difference in hydrogen yield throughout the reaction cycles for PtNPs/$Nb_2O_5 \cdot nH_2O$, with values randomly varying from 69% to 74%. However, in terms of reaction kinetics, there was a consistent decrease in the reaction speed along the assays. Despite this observation, there were no significant differences between the first and second cycles, as well as between the fourth and fifth cycles.

The decrease in the kinetics of the reaction might be explained by the formation of a covering film consisting of strongly adsorbed (poly)borates as suggested by other works.[53,57] Such a film hinders the NPs' surface, decreasing the number of available active sites. The loss of material between manipulations should also be considered as a source for the differences found.

Although the hydrogen yield for the reactions catalyzed by PtNPs/$Nb_2O_5 \cdot nH_2O$ remains consistent across successive cycles, it is noteworthy that the opposite trend is observed when using NiNPs/$Nb_2O_5 \cdot nH_2O$ as catalysts (Fig. 9b). Despite a decrease in the reaction speed over time for both catalysts, for the reasons mentioned above, the latter appears to undergo surface restructuring. This self-optimization may have different reasons, such as improved mixing/mass transfer or simply surface activation induced by the reaction intermediates.[58] This restructuring potentially enhances hydrogen formation and shifts the equilibrium in its favor, despite a reduction in the number of active sites.

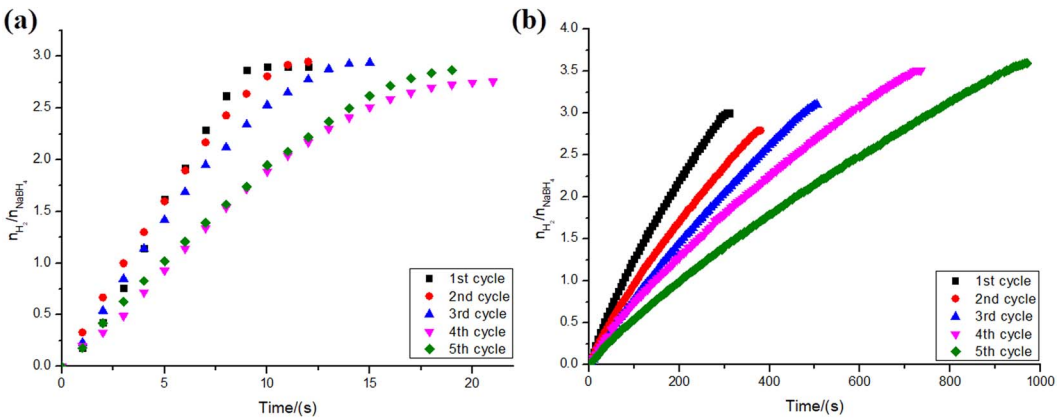

Fig. 9 Reusability assay for $NaBH_4$ hydrolysis using 34.45 μmol of PtNPs (a) and NiNPs (b) over 100 mg of niobic acid (0.5 mmol of $NaBH_4$ in the final volume of 2 mL of type II+ water). The catalyst was washed and vacuum-dried before each reuse (24 ± 1 °C).

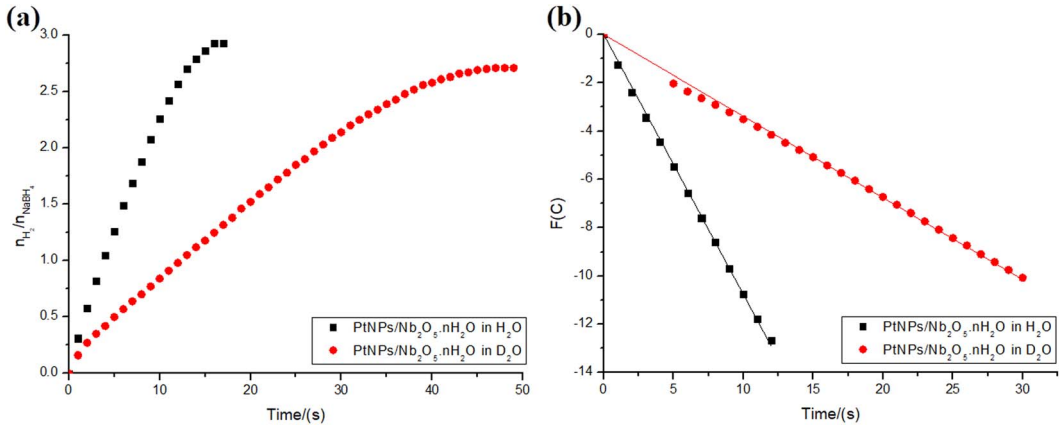

Fig. 10 (a) Hydrogen production ratio with respect to the substrate: 0.5 mmol of $NaBH_4$ in the final volume of 2 mL of type 1 water or deuterated water. The reactions were catalyzed by 34.45 μmol of PtNPs over 100 mg of niobic acid at 22 °C. (b) Kinetic relations for sodium borohydride hydrolysis reactions. Order of both reactions $n = 0.50$. For the reaction in water: $k = 1.1$ mmol^{1-n} L^n s^{-1}, time 0 to 12 s, adjusted $R^2 = 0.9998$. For the reaction in deuterated water: $k = 0.34$ mmol^{1-n} L^n s^{-1}, time 5 to 30 s (including $t = 0$ s), adjusted $R^2 = 0.9996$.

Kinetic isotope effect

The kinetic isotope effect (KIE) provides a means to study the rate-determining step of a reaction. It is calculated by dividing the rate constants obtained for the reaction involving a light isotopically substituted reactant (κ_H) and the one involving a heavy one (κ_D) (KIE = κ_H/κ_D).[38] The effect can be classified as primary if the KIE is between 2–7, and secondary if it falls between 0.7–1.5. In the former case, a bond involving the isotopically labeled atom is formed or cleavaged in the rate-determining step, explaining the significant difference in the rate constant.[38] The latter, however, suggests that there is no bond involving the isotopically substituted atom being cleavaged or formed in the rate-determining step, although it somehow can influence it.[38] The KIE can be explained, for example, by the differences in the vibrational modes of bonds due to the variations in the reduced mass of the system when using a heavier isotope. A higher reduced mass leads to lower vibration frequencies, requiring more energy to reach the transition state.[59]

To investigate whether the rate-determining step in the present hydrolysis of $NaBH_4$ also involves water, the reactions catalyzed by PtNPs/$Nb_2O_5 \cdot nH_2O$ were performed using both water and deuterated water. Only PtNPs were tested in this section, since they displayed better kinetics and no hydrogen yield difference compared to NiNPs (in the 2 mL reaction system). The results are depicted in Fig. 10a. As shown, the use of deuterated water had a significant impact on the reaction kinetics.

To determine the KIE of the reaction, the main kinetic regions were selected for both reactions: 0–12 s for the hydrolysis in water and 5–30 s for the hydrolysis in deuterated water (including the point at $t = 0$ s for the latter, though). The correlations between time and the test function, which were used to determine the kinetic parameters for the reactions, were calculated as described in the ESI† and are depicted in Fig. 10b. To compare both rate constants, the reaction order that best fits one of the data sets was fixed for both ($n = 0.50$). The rate constants were found as 1.1 and 0.34 mmol$^{0.50}$ L$^{0.50}$ s^{-1}, for the reactions in water and deuterated water, respectively. This corresponds to a KIE = 3.2, indicating a primary isotope effect.[38]

While part of the difference in the rate constants could be explained by variations in the stabilization provided by the solvent to the transition state, the primary isotope effect indicates that, indeed, the reaction step involving water corresponds to the rate-determining step of the overall reaction.

To rationalize what might be happening throughout the reaction, it is important to keep in mind that H_2O molecules can be easily activated on noble metals.[38] In the rate-determining step, water molecules may be adsorbed onto the nanometals' surface and activated.[38] The reaction of $NaBH_4$ on PtNPs forms Pt–H in which the H atom is hydridic. This hydrogen then interacts with a hydrogen of water by hydrogen bonding, provoking a weakening of the H–OH bond, which significantly contributes to its cleavage. It cannot be forgotten, however, as was already demonstrated, that the reaction mechanism changes in the course of the reaction due to, among other things, the changes in sodium borohydride concentrations. That being said, it seems that the activation of water molecules remains the rate-determining step, regardless of the mechanism.

Conclusions

This study investigated $NaBH_4$ hydrolysis using Pt, Ni, Pd, and Au nanoparticles stabilized by niobic acid. The new use of the Nb_2O_5 polymorph in sodium borohydride hydrolysis demonstrated a synergistic effect in hydrogen production due to its Brønsted acidity. PtNPs/$Nb_2O_5 \cdot nH_2O$ stood out as the most effective catalyst, revealing concentration-dependent changes in the hydrolysis mechanism. The kinetic isotope assay showed a primary isotope effect, indicating that the cleavage of a H–O bond of water continues to be the slowest step in the reaction mechanism. Reusability assays resulted in sustained yields over five cycles, with a decline in efficiency attributed to reaction

byproducts. The results were modest in comparison with other supports but enriched our knowledge of the properties of niobic acid and expanded the sample space of the materials investigated for sustainable hydrogen production.

Declaration of use of AI-assisted technologies

During the preparation of this work the authors used LanguageTool, Grammarly, and ChatGPT to improve readability and language.

Conflicts of interest

There are no conflicts to declare.

Acknowledgements

This work was supported by the Coordenação de Aperfeiçoamento de Pessoal de Nível Superior – Brazil (CAPES) [grant numbers 312400/2021-7]; the Conselho Nacional de Desenvolvimento Científico e Tecnológico (CNPq) [grant number 405828/2022-5]; the Fundação de Amparo à Pesquisa do Estado de Minas Gerais (FAPEMIG) [FAPEMIG RED-00144-22 and FAPEMIG APQ-01275-18]. The first author also thanks for the doctoral stay grant by CAPES (Brazil) at the Institut des Sciences Moleculaires, University of Bordeaux, Talence, France, where he developed part of this research (Edital no. 44/2022, financial code 001). We acknowledge the support of the University of Bordeaux and the Centre National de la Recherche Scientifique (CNRS). Special recognition goes to the Department of Chemistry and the Department of Physics at Universidade Federal de Viçosa for their support, as well as the Center of Microscopy at Universidade Federal de Minas Gerais (**https://www.microscopia.ufmg.br**) for their technical support.

References

1 National Research Council, *Climate Change: Evidence and Causes: Update 2020*, The National Academies Press, Washington, DC, 2020, vol. 34.
2 K. Ravindra, A. Goyal and S. Mor, *The Lancet Regional Health – Southeast Asia*, 2023, **15**, 100238.
3 M. Z. Jacobson, W. G. Colella and D. M. Golden, *Science*, 2005, **308**, 1901.
4 World Health Organization, *WHO Global Air Quality Guidelines. Particulate Matter (PM25 and PM10), Ozone, Nitrogen Dioxide, Sulfur Dioxide and Carbon Monoxide*, 2021, p. 360.
5 S. M. Hartinger, M. Yglesias-González, L. Blanco-Villafuerte, *et al.*, *The Lancet Regional Health – Americas*, 2023, **20**, 100470.
6 R. Vilcassim and G. D. Thurston, *EBioMedicine*, 2023, **93**, 104668.
7 J. Andersson and S. Grönkvist, *Int. J. Hydrogen Energy*, 2019, **44**, 11901.
8 F. Eljack and M. K. Kazi, *Frontiers in Sustainability*, 2020, **1**, 616762.
9 Y. Sun, R. F. DeJaco, Z. Li, *et al.*, *Sci. Adv.*, 2021, **7**, eagb3983.
10 (*a*) W. Chen, J. Shen, Y. Huang, *et al.*, *ACS Sustain. Chem. Eng.*, 2020, **8**, 7513; (*b*) C. Wang, Q. Wang, F. Fu and D. Astruc, *Acc. Chem. Res.*, 2020, **53**, 2483–2493; (*c*) C. Wang and D. Astruc, *Chem. Soc. Rev.*, 2021, **50**, 3437.
11 S. Akbayrak and S. Özkar, *Int. J. Hydrogen Energy*, 2018, **43**, 18592.
12 (*a*) N. Kang, R. Djeda, Q. Wang, *et al.*, *ChemCatChem*, 2019, **11**, 2341; (*b*) D. Astruc, *Chem. Rev.*, 2020, **120**, 461.
13 (*a*) H. C. Brown, *Organic Syntheses via Boranes*, John Wiley & Sons, Inc., New York, 1975; (*b*) J. Seyden-Penne, *Reductions by the Alumino- and Borohydrides in Organic Synthesis*, VCH-Lavoisier, Paris, 1991.
14 D. Astruc, F. Lu and J. Ruiz, *Angew. Chem., Int. Ed.*, 2005, **44**, 7852.
15 C. Deraedt, L. Salmon, S. Gatard, R. Ciganda, R. Hernandez, J. Ruiz and D. Astruc, *Chem. Commun.*, 2014, **50**, 14194.
16 P. Michaud, D. Astruc and J. H. Ammeter, *J. Am. Chem. Soc.*, 1982, **104**, 3755.
17 H. I. Schlesinger, H. C. Brown, A. E. Finholt, J. R. Gilbreath, *et al.*, *J. Am. Chem. Soc.*, 1953, **75**, 215.
18 (*a*) N. A. Choudhury, R. K. Raman, S. Sampath and A. K. Shukla, *J. Power Sources*, 2005, **143**, 1; (*b*) U. B. Demirci, O. Akdim, J. Andrieu, *et al.*, *Fuel Cells*, 2010, **10**, 335; (*c*) L. Yu and M. A. Matthews, *Int. J. Hydrogen Energy*, 2011, **36**, 7416; (*d*) T. He, P. Pachfule, H. Wu, Q. Xu and P. Chen, *Nat. Rev. Mater.*, 2016, **1**, 16059.
19 C. Luo, F. Fu, X. Yang, *et al.*, *ChemCatChem*, 2019, **11**, 1643.
20 M. Farrag and G. A. M. Ali, *Sci. Rep.*, 2022, **12**, 17040.
21 H. Jafarzadeh, C. Karaman, A. Güngör, *et al.*, *Chem. Eng. Res. Des.*, 2022, **183**, 557.
22 A. Paksoy, S. F. Kurtoğlu-Öztulum, M. B. Yağcı and Ö. Balcı-Çağıran, *Int. J. Hydrogen Energy*, 2022, **47**, 36898.
23 C. Gao, F. Lyu and Y. Yin, *Chem. Rev.*, 2021, **121**, 834.
24 R. P. Lopes and D. Astruc, *Coord. Chem. Rev.*, 2021, **426**, 213585.
25 M. Tarselli, *Nat. Chem.*, 2015, **7**, 180.
26 A. R. Alves and A. dos R. Coutinho, *Miner. Eng.*, 2019, **132**, 275.
27 V. Lacerda Jr, D. A. dos Santos, L. C. da Silva-Filho, *et al.*, *Aldrichimica Acta*, 2012, **45**, 19.
28 C. Zhang, M. Beidaghi, M. Naguib, *et al.*, *Chem. Mater.*, 2016, **28**, 3937.
29 I. D. Ivanchikova, I. Y. Skobelev, N. V. Maksimchuk, *et al.*, *J. Catal.*, 2017, **356**, 85.
30 P. M. Monte, A. P. P. M. da Silva, L. Fortes, *et al.*, *Rev. Virtual Quim.*, 2021, **13**, 1391.
31 A. Islam, S. H. Teo, Y. H. Taufiq-Yap, *et al.*, *J. Cleaner Prod.*, 2021, **318**, 128439.
32 C. Zhou, R. Shi, G. I. N. Waterhouse and T. Zhang, *Coord. Chem. Rev.*, 2020, **419**, 213399.
33 K. Tanabe, *Mater. Chem. Phys.*, 1987, **17**, 217.
34 K. Nakajima, Y. Baba, R. Noma, *et al.*, *J. Am. Chem. Soc.*, 2011, **133**, 4224.
35 Y. Zhao, X. Zhou, L. Ye and S. C. E. Tsang, *Nano Rev.*, 2012, **3**, 17631.

36 D. Stošić, S. Bennici, V. Pavlović, *et al.*, *Mater. Chem. Phys.*, 2014, **146**, 337.
37 M. M. C. Fraga, J. Vogt, B. L. de O. Campos, *et al.*, *Energy Fuels*, 2023, **37**, 10474.
38 Z. Li, T. He, L. Liu, *et al.*, *Chem. Sci.*, 2016, **8**, 781.
39 (*a*) P. Yan, S. Xi, H. Peng, *et al.*, *J. Am. Chem. Soc.*, 2023, **145**, 9718; (*b*) D. Drobot, E. Nikishina, E. Lebedeva, *et al.*, *Mater. Res. Bull.*, 2008, **43**, 1232.
40 R. Retnamma, A. Q. Novais and C. M. Rangel, *Int. J. Hydrogen Energy*, 2011, **36**, 9772.
41 J. M. Jehng and I. E. Wachs, *Chem. Mater.*, 1991, **3**, 100.
42 L. R. V. da Conceição, L. M. Carneiro, J. D. Rivaldi and H. F. de Castro, *Ind. Crops Prod.*, 2016, **89**, 416.
43 A. Levy, J. B. Brown and C. J. Lyons, *Ind. Eng. Chem.*, 1960, **52**, 211.
44 Y. C. Lu, M. S. Chen and Y. W. Chen, *Int. J. Hydrogen Energy*, 2012, **37**, 4254.
45 N. P. Ghodke, S. Rayaprol, S. V. Bhoraskar, *et al.*, *Int. J. Hydrogen Energy*, 2020, **45**, 16591.
46 Y. Wang and X. Liu, *ACS Appl. Nano Mater.*, 2021, **4**, 11312.
47 (*a*) G. Sperandio, I. M. Junior, E. Bernardo, *et al.*, *Processes*, 2023, **11**, 3250; (*b*) I. Machado Junior, G. H. Sperandio and R. P. Lopes, *Int. J. Hydrogen Energy*, 2023, **53**, 1323.
48 V. G. Minkina, S. I. Shabunya, V. I. Kalinin, *et al.*, *Int. J. Hydrogen Energy*, 2012, **37**, 3313.
49 S. Ilic, A. Alherz, C. B. Musgrave and K. D. Glusac, *Chem. Soc. Rev.*, 2018, **47**, 2809.
50 M. C. Daniel and D. Astruc, *Chem. Rev.*, 2004, **104**, 293.
51 Q. Quach, E. Biehler, A. Elzamzami, *et al.*, *Catalysts*, 2021, **11**, 118.
52 C. Huff, J. M. Long, A. Heyman and T. M. Abdel-Fattah, *ACS Appl. Energy Mater.*, 2018, **1**, 4635.
53 U. B. Demirci and P. Miele, *C. R. Chim.*, 2014, **17**, 707.
54 S. Doherty, J. G. Knight, H. Y. Alharbi, *et al.*, *ChemCatChem*, 2022, **14**, e202101752.
55 J. Zhang, T. S. Fisher, J. P. Gore, *et al.*, *Int. J. Hydrogen Energy*, 2006, **31**, 2292.
56 A. H. Hatta, A. A. Jalil, N. S. Hassan, *et al.*, *Int. J. Hydrogen Energy*, 2022, **47**, 30981.
57 J. H. Kim, K. T. Kim, Y. M. Kang, *et al.*, *J. Alloys Compd.*, 2004, **379**, 222.
58 Y. Zhang, J. Pan, G. Gong, *et al.*, *Catalysts*, 2003, **13**, 120.
59 E. V. Anslyn and D. A. Dougherty, *Modern Physical Organic Chemistry*, University Science Books, 2006.